Available online at www.sciencedirect.com

ScienceDirect

International Journal of Naval Architecture and Ocean Engineering 8 (2016) 177–187
http://www.journals.elsevier.com/international-journal-of-naval-architecture-and-ocean-engineering/

Tractive performance evaluation of seafloor tracked trencher based on laboratory mechanical measurements

Meng Wang [a], Xuyang Wang [a,*], Yuanhong Sun [b], Zhimin Gu [b]

[a] School of Naval Architecture, Ocean and Civil Engineering, Shanghai Jiaotong University, Shanghai, 200240, China
[b] North China Sea Marine Technical Support Center, State Oceanic Administration, Qingdao, 266061, China

Received 6 October 2015; revised 23 November 2015; accepted 25 January 2016
Available online 13 March 2016

Abstract

To evaluate the tractive performance of tracked trencher on seafloor surface, a new shear stress-displacement empirical model was proposed for saturated soft-plastic soil (SSP model). To validate the SSP model, a test platform, where track segment shear test can be performed in seafloor soil simulacrum (bentonite water mixture), was built. Series shear tests were carried out. Test results indicate that the SSP model can describe the mechanical behavior of track segment with good approximation in seafloor soil simulacrum. Through analyzing the main external forces applied to seafloor tracked trencher during the uniform linear trenching process, a drawbar pull prediction model was deduced with the SSP model. A tracked walking mechanism of the seafloor tracked trencher prototype was built, and verification tests were carried out. Test results indicate that this prediction model was feasible and effective; moreover, from another side, this conclusion also proved that the SSP model was effective.

Keywords: Shear stress-displacement relationship; SSP model; Tractive performance; Drawbar pull; Seafloor tracked trencher

1. Introduction

With growing demand for offshore wind energy, the number of seafloor cables required to export energy from wind farms to shore has also increased in recent years (Royal Haskoning and BOMEL Ltd, 2008). As a result, large number of cables associated with energy delivery and telecommunications will be installed during the coming decades. Sometimes seafloor cables cross busy shipping routes, fishing areas where the seafloor is frequently disturbed by dredging, trawling and anchoring. The seafloor cables may be damaged when exposed on seafloor surface, and thus, these cables need proper protection. To reduce the risk of damaging cables, effective cable protection, careful execution of cable laying and burial operations are required. Cable burial is a preferred way to protect cables against these impacts. Seafloor trenching is usually done by equipments mounted on a seabed carriage or sled, which may be either self-propelled or towed. Seafloor Tracked Trencher (STT) equipped with jetting system is designed to meet the burial requirements of pipelines and cables above-mentioned.

STT's mobility requires both sufficient traction and bearing capacity. The working capacity depends principally on vehicle dimensions and seafloor soil property. Tracked walking mechanism has a larger contact area with ground than wheeled running gear, so, it can provide better floatation and larger traction forces. By shearing seafloor surface soil, tracks can produce traction force that propels the trencher forward, and the available traction must be sufficient to enable trencher to overcome various resistances, including vehicle weight due to slope/vehicle pitch and compaction resistance which arises as a consequence of creation of ruts.

* Corresponding author.
E-mail address: c_ranger@126.com (X. Wang).
Peer review under responsibility of Society of Naval Architects of Korea.

http://dx.doi.org/10.1016/j.ijnaoe.2016.01.005 / pISSN : 2092-6782, eISSN : 2092-6790

Trafficability evaluation of the seafloor surface and potential traction optimization of the tracked walking mechanism are essential and some research works have been done. Through experiments analysis, Janosi and Hanamoto (1961) proposed a drawbar pull model as a function of slip for a tracked vehicle in deformable soils. Watanabe and Kitano (1986) presented a theoretical and experimental analysis of steering performance of articulated tracked vehicles on level ground, and developed a mathematical model for predicting the steerability of articulated units. Considering possible factors related to steering problems such as track slippage, centrifugal force and vehicle configuration, Kitano and Jyozaki (1976) developed a steering model for uniform turning motion and steerability in plane motion of vehicles. Baladi and Rohani (1978), have studied and developed the application of tracked vehicles on soft soil. Hyung-Woo Kim (2005) analyzed underwater tracked vehicle's dynamics on extremely soft soil by using Euler Parameters and investigated the hydrodynamic effects on the performance of tracked vehicle. Based on deep sea soil situ measurements and bentonite soil laboratory tests, Schulte (2001) developed a shear stress-displacement relationship function for deep sea soil. This function fits measurement result of segment shear test well in descending part and residual part; but in the hump part, the calculated curves appears some deviations, and there exists an offset for $s = 0$.

In this paper, based on comprehensive analyses of seafloor soil shear deformation and the track segment shear tests, a new shear stress-displacement relationship empirical model was proposed for saturated soft-plastic soil (SSP model). To verify the SSP model, a test platform, in which track segment shear test can be performed in seafloor soil simulacrum (bentonite water mixture), was designed and built. Series of track segment shear tests are carried out. Through analyzing the main external forces, including environmental loads from the seafloor soil and current applied to tracked trencher during the uniform linear trenching process, a drawbar pull prediction model was deduced with SSP model. At last, for validating this prediction model, drawbar pull tests were carried out with a tracked walking mechanism of STT prototype.

2. Mechanics of track–soil interaction

The attainable locomotion of the STT over seafloor surface is mainly based on shear forces which are developed by track segments shearing soil surface in longitudinal directions of track links. So, seafloor surface soil conditions have significantly effects on tractive performance to tracked trenchers. The mechanical behavior of surface soil varies considerably under a wide variety of environmental conditions. For example, composition, moisture levels and porosity affect mechanical behavior of bulk soil relative to vehicle/terrain dynamics. Some experiments indicated that the shear behavior of seafloor surface sediments shows a similar behavior as a type of "undisturbed firm soil" (Kim et al., 2005; Schulte et al., 2001; Wu and He, 2010). As shown in Fig. 1, this type of soil exhibits characteristics as follows described, shear stress initially increased sharply and reached a "hump" of maximum shear stress (τ_{max}) at a particular shear displacement, and then decreased and approached a relative constant residual value (τ_{res}) with further increase in shear displacement.

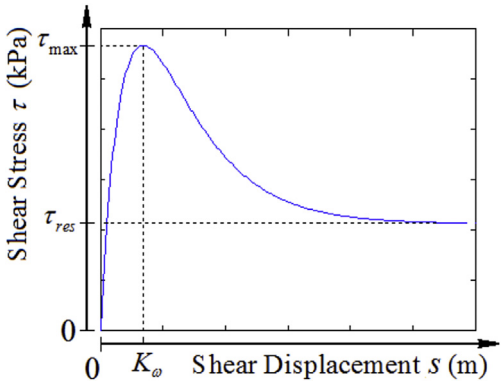

Fig. 1. Shear curve exhibiting a peak and constant residual shear stress.

2.1. Physical and mechanical characteristics of seafloor surface soil

The physical and mechanical characteristics of seafloor surface soil are special. With the increase of depth, the soil mass presents flow state, fluidal plastic state, and plastic state (Enderby, 1974). Elastic-plastic deformation may play an important role in track segment shearing process. Taking surrounding soil deformation of track segment into account, the schematic diagram of soil deformation can be shown as Fig. 2-a. The deformation is not linear. The influence zone (D_w, D_h) depends on many factors, such as normal stress (σ), soil cohesion (c), soil internal friction angle (ϕ), shear deformation modulus (K), soil moisture content (w), etc. A typical shear process can be described as follows: at the beginning, the shear stress increases proportionally to the shear displacement, indicating that the soil is deformed mostly elastic; at a certain shear displacement, the soil starts to fail and plastic deformation occurs, the shear bock starts to form; when the maximum shear stress is reached, the soil is completely broken; after this, the shear stress declines to its residual value; but the soil mass under shear bock is still in deformation state caused by frictional effects. As shown in Fig. 2-b, it was not difficult to observe the deformation process above-mentioned during the shear tests.

Through analyzing the test data, it's very interesting to find that the hump zone energy loss ΔE_H seems to be caused mainly by elastic–plastic deformation of the shear bock and the soil mass around track segment, and the residual zone loss ΔE_R can be considered as energy loss caused by friction of the soil mass around track segment. And these two types of energy losses seem to be independent from each other. Therefore, here, when analyzing and modifying the shear stress-displacement model, these two types of energy losses are considered and modified independently. The mechanical behavior analysis of seafloor soil shear deformation and theoretical derivation of shear stress-displacement model are

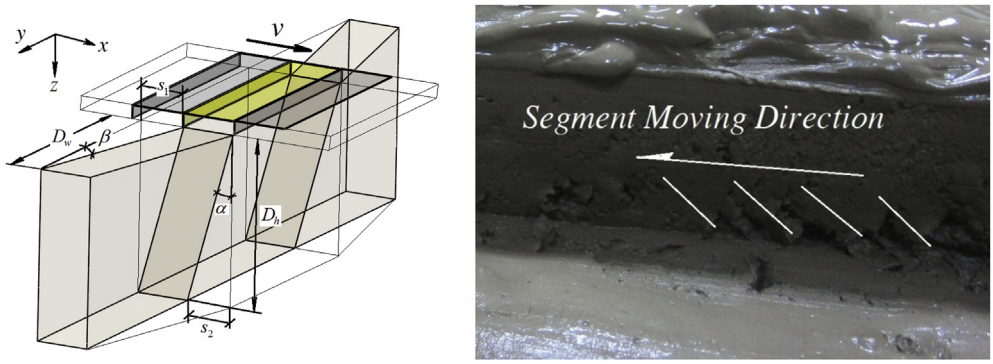

(a) (b)

Fig. 2. Soil mass deformation during track segment shear test.

not the study focus of this paper, and they will be discussed in detail in the future.

On the basis of early track segment shearing tests and comprehensive analysis above-mentioned, a new empirical model for saturated soft-plastic soil shear stress-displacement (SSP model) is introduced as follows,

$$\tau = k_{pm}\cdot\left[-\left(e^{-s/K_\omega}-c_{pm}\right)^2+\left(1-c_{pm}\right)^2\right]\cdot\tau_{\max} + k_{pr}\cdot\left[\left(e^{-s/K_\omega}-c_{pr}\right)^2-\left(1-c_{pr}\right)^2\right]\cdot\tau_{res} \quad (1)$$

where, τ_{max} is the maximum shear stress of a contact area and can be measured for the test curves, or be calculated by Mohr-Coulomb equation; τ_{res} is the residual shear stress; K_ω is the shear displacement where the maximum shear stress τ_{max} occurs; c_{pm} is the correction factor caused by the soft-plastic deformation loss in hump zone; c_{pr} is the correction factor caused by the soft-plastic deformation loss in residual zone; k_{pm} is the adjustment coefficient of the hump part; k_{pr} is the adjustment coefficient of the residual part.

It is not difficult to fit this function according to the measured values, as the parameters are almost independent from each other. The values of τ_{max}, τ_{res}, K_ω can be directly identified from the measured shear curve. The values of c_{pm} and c_{pr} can be calculated according to the least square error. Through the analysis of the track segment tests, it was found another interesting phenomena that the values of c_{pm}, c_{pr} changed little for the bentonite-water mixture with different water content and different vertical pressure, and the values of k_{pm} and k_{pr} are nearly constant values. The parameter values above-mentioned obtained from early shearing tests are shown in Table 1.

Table 1
Parameter values of SPP model calculated from test results.

Parameter	Value
Correction factor of hump zone soft-plastic deformation loss (c_{pm})	0.51
Correction factor of residual zone soft-plastic deformation loss (c_{pr})	0.68
Adjustment coefficient of hump zone (k_{pm})	4.30
Adjustment coefficient of residual zone (k_{pr})	2.72

2.2. Test platform

A test platform (Fig. 3) was designed to carry out track segment shearing tests and plate pressure-sinkage tests. The test platform is equipped with a linear speed control module to ensure the linear speed of the track segment shear movement, and this test platform is also equipped with a vertical loading device to adjust contact pressure (p_v) between track segment and soft soil. Technical details of the test platform are shown in Table 2.

Soil conditions can affect tractive performance of the tracked vehicles, some test results have proved this effect and these tests indicated that soil property is an important factor to the prediction or analysis of track–soil interaction (Bekker, 1960; Upadhyaya et al., 1989). Bentonite water mixtures shows to be acceptable deep sea soil substitutes, as the material composition and the main characteristics are similar (Li and Shulin, 2010). So, here, bentonite water mixture is used as the seafloor soil simulacrum. It is very hard to simulate the maximum and residual shear strengths of the seafloor soil simultaneously, so here, only residual shear strength was aimed (Li and Shulin, 2010). The shear strength of mixture is controlled by water content. To insure the shear strength of mixture well-distributed, the water content of soil should be maintained uniformly. After each set of measurements, the bentonite-water mixture is thoroughly mixed with a mixing device and left to stand still for some days. To ensure accuracy and adjustability of contact pressure between track segment and bentonite water mixture, lead blocks and steel grits are used as the loading weights.

2.3. Shear stress-displacement measurements with track segment

During track segment shear testing, three simplified track segments with grousers distributed equidistantly underneath are put on top of the mixture. The middle track segment can move freely in horizontal movement direction and is fastened on the bottom of six-axis force/torque transducer as shown in Figs. 3 and 4. Vertical loading device applies pressure on the middle track segment. Six-axis force/torque transducer (SI-475-20) and data-acquisition module (NET F/T 9105) were

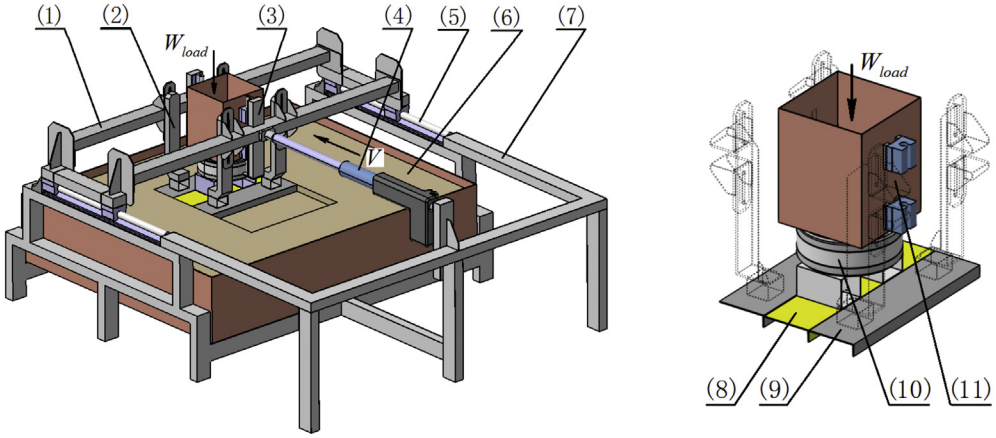

(1) horizontal sliding beams; (2) front and rear plate support; (3) vertical linear guide rail; (4) linear motion actuator; (5) horizontal linear guide rail; (6) soil bin; (7) main frame; (8) middle test plate; (9) front plate and rear plate; (10) six-axis force/torque transducer; (11) loading weight box

Fig. 3. Overview of the test platform.

Table 2
Technical details of the test platform.

Soil bin inner dimensions	Length − 2 m; Width − 1.5 m; Depth of bentonite − 0.8 m
Shear velocity	Up to 0.05 m/s
Test conditions	Undrained; With free sinkage or without free sinkage
Test item 1	Shear stress − Displacement relationship
Test item 2	Pressure−Sinkage Relationship
Sample segment 1	Length − 0.4 m; Width − 0.1 m; Grouser height − 0.05 m
Sample segment 2	Length − 0.6 m; Width − 0.15 m; Grouser height − 0.1 m

used to measure the shear force applied to middle track segment and vertical pressure applied by the loads; and according to shearing velocity, sampling frequency was set at 20 sample per second. The front and rear plates are fixed to eliminate front and rear effects.

Series tests are carried out with two groups of simplified track segments with different sizes (Table 2, Fig. 4). Each shearing test was performed three times to obtain effective values. By applying vertical pressure (p_v), dynamic sinkage can occur freely during the middle track segment traveling through the test area. The shear force (F_S) caused by middle segment is measured via six-axis force/torque transducer. The shear stress can be calculated by dividing shear force with the shear area of middle test plate. So, the shear stress τ caused by the middle plate can be calculated as follows,

$$\tau = \frac{F_S}{A_m} = \frac{F_S}{l \cdot (b + 2h)} \tag{2}$$

where F_S is the shear force; A_m is the shearing area between middle track segment and bentonite water mixture, and $A_m = l \cdot (b + 2h)$; b is the smaller dimension of the test segment; l is the long dimension of the test segment; h is the grouser height.

Several track segment shear tests were conducted with different water content (w_c) and different vertical contact pressure (p_v). Test results are shown in Figs. 5 and 6. During the shearing process, it was found that the assembling clearance between vertical linear guide rail and loading weight box was slightly larger, and this led to large fluctuations in measured curve, as shown in Fig. 5. After adjusting assembling clearance, this problem was solved.

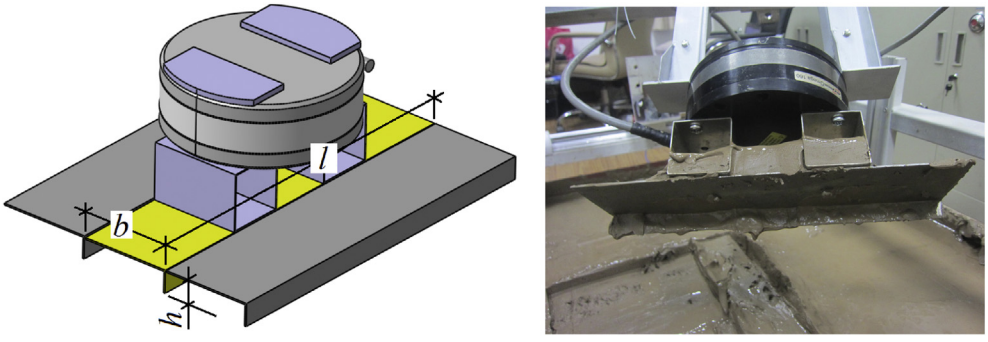

(a) (b)

Fig. 4. The middle test plate fastened on the bottom of six-axis force/torque transducer.

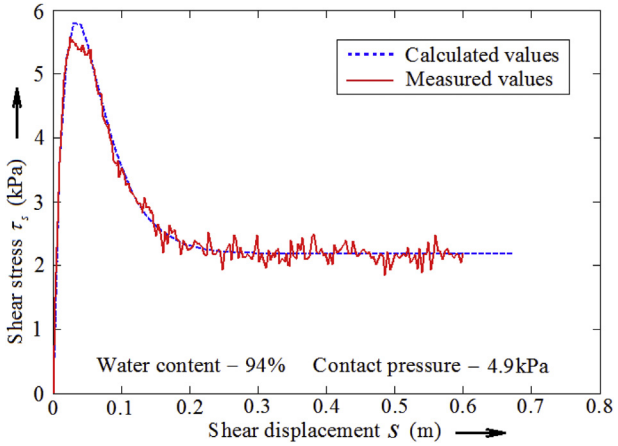

Fig. 5. Shear stress-displacement measured curve with track segment in comparison with calculated curve according to SSP model (w_c = 94%, p_v = 4.9 kPa).

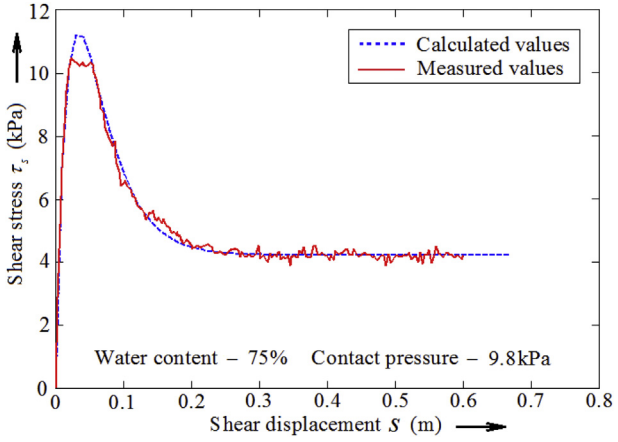

Fig. 6. Shear stress-displacement measured curve with track segment in comparison with calculated curve according to SSP model (w_c = 75%, p_v = 9.8 kPa).

As measured curves shown in Figs. 5 and 6, shear stress initially increased rapidly with the increase of shear displacement at first, and shear stress reached a larger value range at some deformation, then dropped to a lower constant value as deformation increasing. Due to test conditions, measured curves displayed some fluctuations, and peak values weren't achieved. These phenomena may be caused by the insufficient stiffness of sliding beams and assembling clearance (Fig. 3). But overall, the prediction curves calculated according to SSP model fit the measured curves well. So, the SSP model can describe the mechanical behavior of track segment with good approximation in seafloor soil simulacrum.

3. Tractive performance

During the linear trenching process, main external forces, including environmental loads from seafloor soil and sea current applied to STT, are shown in Fig. 7. F_T is the tractive force produced by track segments shearing seafloor surface soil; F_B is the buoyant force; F_{HD} is the hydrodynamic force;

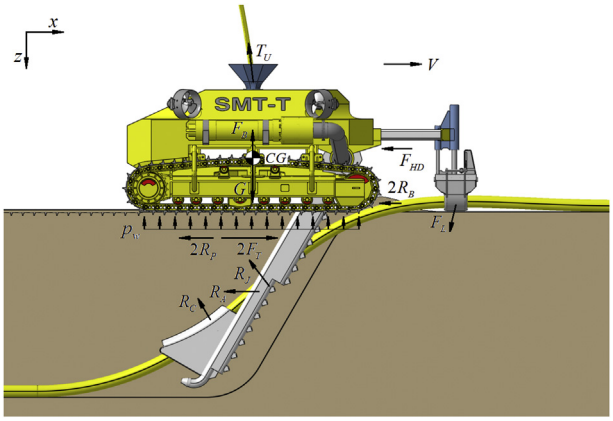

Fig. 7. Main external forces acting on seafloor tracked trencher.

R_P, R_A, R_B, R_J are compaction resistance, friction resistance between jet arm and trench wall, bulldozing resistance, and jetting reaction force respectively; R_C and F_L are cable restraining resistances; T_U is the umbilical drag force. p_w is the working contact pressure between track segments and seafloor. These forces can be divided into motion resistances and working resistances; R_P and R_B, which caused by terrain deformation, are usually classified as the motion resistances, and other forces are classified as working resistances. Tracked walking mechanism has to produce an amount of thrust to overcome all working resistances and motion resistances.

With the main forces acting on the seafloor tracked trencher (Fig. 7), the basic motion equation can be set up as follows,

$$\begin{cases} m_T\ddot{x} = 2F_T - 2(R_P + R_B) - (F_{HD} + F_{Lx} + R_A + R_{Cx} + T_{Ux} + R_{Jx}) \\ G = 2Ap_w + (F_B + R_{Cz} + R_{Jz} + T_{Uz} - F_{Lz}) \end{cases} \tag{3}$$

where m_T is inertial mass of the seafloor tracked trencher, G is the trencher weight, $G = m_T \cdot g$; A is the contact area of one-side track; R_{Cx}, R_{Jx}, F_{Lx}, T_{Ux} is the corresponding force component in x-axis; R_{Cz}, R_{Jz}, T_{Uz}, F_{Lz} is the corresponding force component in z-axis.

The tractive performance can be characterized by tractive effort, motion resistances and drawbar pull. Drawbar pull is defined as the difference between total tractive effort (including the thrust developed by vertical shearing surfaces on both sides of the tracks) and the total external motion resistance of the vehicle. It is customary to view drawbar pull as the vehicle's ability to drive both itself and working loads. Assuming that the distribution of working contact pressure is uniform, in accordance with Eq. (3), the drawbar pull prediction model can be written as,

$$\begin{cases} F_D = 2F_T - 2(R_P + R_B) \\ p_w = \dfrac{1}{2A} \cdot W_{Ly} = \dfrac{1}{2A} \cdot \left[G - \left(F_B + R_{Cy} + R_{Jy} + T_{Uy} - F_{Ly}\right)\right] \\ k_M = F_D / \max\{W_{Lx}\} = F_D / \max\{m_T\ddot{x} + \\ \qquad (F_{HD} + F_{Lx} + R_A + R_{Cx} + T_{Ux} + R_{Jx})\} \end{cases} \tag{4}$$

where F_D is defined as the drawbar pull; W_{Ly} is the mean normal working loads acting on the tracks; W_{Lx} is the horizontal working loads acting on the tracks; k_M is defined as the determining factor of operation margin.

It should be noted that the actual motion of STT is sluggish (about 300 m/hr) when trenching, and the acceleration of the trencher is relatively slow too; so, in the design and verification process, the interference of the motion state change to net drag force can be ignored. Within the frame of this paper, $\ddot{x}$ is assigned with zero. Assuming that the soil conditions and working slip of tracks have been obtained from the model test, the drawbar pull F_D can be considered as meeting the design requirements if the calculated value of operation margin factor k_M is greater than or equal 1.3 during engineering design process. In this paper, the working resistances were not involved in drawbar pull calculation and validation tests, so, the derivation and conclusion of working resistances were not provided; but it should be noted that these resistances should be taken into account in the engineering design.

3.1. Traction force calculation

For vehicle performance evaluation, it is desirable to determine the variation of thrust with track slip over the full operating range. The shear displacement at various points beneath a track is shown as Fig. 8. When a certain grouser comes into seafloor soil at the front of a track, shear displacement of soil is zero. Caused by the difference between track belt velocity and vehicle velocity over the terrain, the horizontal shear displacement increases linearly along contact length till grouser leaves soil again, and reaches its maximum value at the rear of the contact area. To examine the development of shear displacement beneath a track quantitatively, the track slip i is defined as,

$$i = 1 - \frac{V_t}{r_S\omega} = \frac{r_S\omega - V_t}{r_S\omega} \tag{5}$$

where V_t is the actual forward speed of track; r_S is the radius of sprocket pitch circle; ω is the angular velocity of rear sprocket.

Since track cannot stretch, the speed of slip $r_S\omega - V_t$ is the same for very point of track in contact surface with the terrain.

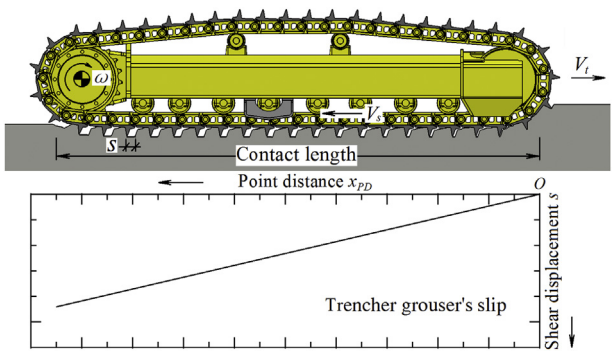

Fig. 8. Shear displacement under a track belt.

Assuming that t is the contact time of the point located at a distance x_{PD} from the front of the track, $t = x_{PD}/r_S\omega$, with Eq. (5), the shear displacement s at a point can be determined by,

$$s = (r_S\omega - V_t)t = i \cdot x_{PD} \tag{6}$$

The main tractive effort developed either by frictional or cohesive forces is related to shear area located beneath the track, and this area is often identified as the ground contact area. Moreover, there are two other additional shear areas per track, which locate along the track sides. Assuming that the grouser depth is denoted by h, the additional areas will amount to $4hs$, and these additional areas cannot be neglected in evaluation of tractive effort.

Making use of the SSP model (Eqs. (1) and (6)), the shear stress at any point of contact area can be determined. Assuming that the normal pressure distributed uniformly, the traction force F_T can be calculated by integrating the shear stress over the soil contact length (L), as follows,

$$F_T = \int_0^L (B+2h)\cdot\left\{k_{pm}\cdot\left[-\left(e^{\frac{-ix}{K_\omega}} - c_{pm}\right)^2 + \left(1-c_{pm}\right)^2\right]\cdot\tau_{\max} + k_{pr}\cdot\left[\left(e^{\frac{-ix}{K_\omega}} - c_{pr}\right)^2 - \left(1-c_{pr}\right)^2\right]\cdot\tau_{res}\right\}\cdot dx \tag{7}$$

where L is the contact length between track and seafloor surface soil, B is the track width.

Solving the integral equation (Eq. (7)), the traction force F_T can be expressed as,

$$F_T = k_{pm}\cdot\left\{\frac{K_\omega}{2iL}\left(e^{\frac{-iL}{K_\omega}} - 2c_{pm}\right)^2 - \left(2c_{pm}-1\right)\left[1+\left(2c_{pm}-1\right)\frac{K_\omega}{2iL}\right]\right\}\cdot(B+2h)L\cdot\tau_{\max} + k_{pr}\cdot\left\{-\frac{K_\omega}{2iL}\left(e^{\frac{-iL}{K_\omega}} - 2c_{pr}\right)^2 + \left(2c_{pr}-1\right)\left[1+\left(2c_{pr}-1\right)\frac{K_\omega}{2iL}\right]\right\}\cdot(B+2h)L\cdot\tau_{res} \tag{8}$$

3.2. Motion resistance

When a tracked vehicle crosses a particular piece of terrain, it will undergo some sinkage which is dependent upon the pressure–sinkage relationship of terrain, track dimensions and weight of the vehicle. Fig. 9-(a) shows the variable remoulding process of soil below tracks and ruts creating. The visible effect of this process is the creation of ruts as the STT travels across the seafloor surface, as shown in Fig. 9-(b). This type of resistance is referred in terramechanics as “compaction resistance”. Bekker (1969) suggested that the doing work by normal reaction exerted on track by terrain can be equated to that done by a pressuring plate reaching the same depth in pressure-sinkage test, and this type of sinkage is usually described as “static pressure sinkage”. On the other hand, the tracklayers developed an

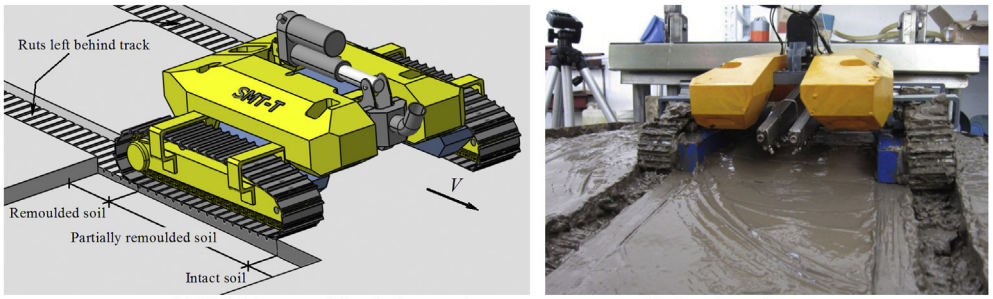

(a) Variable remoulding below tracks (b) Creation of ruts

Fig. 9. Variable remoulding below tracks and creation of ruts.

increasing sinkage with increasing slip, this often occurred at the back of track causing tail down attitude, and can be seen in the field. Reece advised that this type of sinkage, described as "slip sinkage", should be taken into account; the analysis of slip sinkage effect on tractive performance in different soils has shown that this effect cannot be ignored (Reece, 1965). As shown in Fig. 9-(b), the static pressure sinkage and the slip sinkage effect are not difficult to be observed in the traveling tests.

Assuming that the work done by compacting seafloor soil and making a rut ($B \times L \times z_0$), is equated to the motion work done in making a rut of length L with equivalent resistance R_P. The equivalent resistance R_P can be written as,

$$R_P = R_S + R_I \tag{9}$$

where R_S the is the resistance caused by the static pressure sinkage; R_I is the resistance caused by the slip sinkage effect.

3.2.1. Static pressure sinkage resistance

With pressure–sinkage equation proposed by Bekker (1969), the relationship of static pressure sinkage z and soil pressure p can be written as,

$$z = \left(\frac{p}{k_c/b + k_\phi}\right)^{\frac{1}{n}} \tag{10}$$

where k_c is the cohesive soil modulus; k_ϕ is the friction soil modulus; n is the soil deformation exponent.

According to Eq. (10), the final static pressure sinkage z_S caused by working contact pressure p_w can be determined as,

$$z_S = \left(\frac{p_w}{k_c/b + k_\phi}\right)^{\frac{1}{n}} \tag{11}$$

R_S can be determined by,

$$BL \cdot \int_0^{z_S} p dz = R_S L \tag{12}$$

Solving equations (Eqs. (10)–(12)), the equivalent motion resistance R_S can be expressed as,

$$R_S = \frac{B}{(n+1)\cdot(k_c/B + k_\phi)^{1/n}} \cdot (p_w)^{(n+1)/n} \tag{13}$$

3.2.2. Slip sinkage resistance

To precisely predict the sinkage and external motion resistance of a vehicle in a given soil and operating conditions, the slip sinkage effect should be taken into account. Reece (Reece, 1965) advised to use the following formula to evaluate the slip sinkage due to the soil horizontal deformation.

$$Z_I = \frac{h \cdot i}{1 - i} \tag{14}$$

where z_I is the slip sinkage due to soil horizontal deformation, and the varying range of slip is 0–0.8.

Eq. (14) shows that the additional sinkage is originally small, but at slip $i = 0.5$, it reaches the height of the grouser h. It's very difficult to separate slip sinkage z_I from static sinkage z_S, the verification test cannot be done. From the conservation of energy viewpoint, vertical work done in compacting of the soil can be equated to the motion work done in making a rut of length L with equivalent resistance R_I,

$$p_w A \cdot z_I = R_I L \tag{15}$$

where R_I is the equivalent resistance caused by slip sinkage.

With Eqs. (14) and (15), R_I can be deduced as,

$$R_I = \frac{p_w A h \cdot i}{L(1 - i)} \tag{16}$$

3.2.3. Bulldozing resistance

On soft terrain where vehicle sinkage is obvious and significant, Bekker suggested that bulldozing resistance acting in front of the track should be taken into account (Wong and Preston-Thomas, 1983). Bulldozing is the accumulation of soil mass in front of a vehicle. The total bulldozing resistance may be computed using earth pressure theory,

$$R_B = b\left(0.67 h_P c \cdot K_c + 0.5 z^2 \gamma \cdot K_\gamma\right) \tag{17}$$

where, h_P is the height of the pushing soil; c is the soil cohesion; γ is the soil density; K_c is the modulus of cohesion of soil deformation; K_γ is the modulus of density of soil deformation.

It should be noted that the pushing soil was not obviously observed in front of the tracks in the actual drawbar pull test (Fig. 12); so, in this paper, bulldozing resistance was ignored, and the bulldozing resistance R_B is assigned with zero during the draw bar pull calculation. But, it should be noted that bulldozing resistance should be taken into account if the pushing soil can be obviously observed in front of the tracks.

3.3. Drawbar pull test

3.3.1. Overviews of STT prototype

Three-dimensional model of STT is shown as Fig. 10. General characteristics are shown in Table 3, and the principal dimensions are given in Table 4. Four counterweight supports are set up in four corners of the chassis. Steel ingots are used as the counterweights. By increasing or decreasing counterweights, contact pressure and pressure distribution can be adjusted to meet the test requirements.

3.3.2. Test solutions

As can be seen from Eq. (8), the traction force F_T is a function of the slip i. When the tracked walking mechanism is moving uniformly in straight line with speed v and angular velocity ω of rear sprocket, the slip i can be considered as a constant value according to Eq. (5); and this provides possibility for verification tests.

As shown in Fig. 11, drawbar pull tests will be performed in a test soil pool (Length-40 m, Width-8m, Depth-1.5 m), in which is filled with the soil taken from coastal beach; and drawbar pull tests are conducted with the tracked walking mechanism of STT prototype. One fork truck and one wheel loader (Fig. 2) are used as the mechanical adjustable damping; by adjusting brake gear, the fork truck can provide about 10–50 kN drag resistance; the wheel loader can produce about 30–100 kN drag resistance. The slip of STT is calculated by counting the pulses from three encoders; one encoder is connected at the cable length meters (Fig. 11-(5)); and two encoders are fixed on rear sprockets of tracks (Fig. 11-(8)). Drawbar pull force is measured by tension sensor (Fig. 11-(7)); one side of the tension sensor is connected at the end of towing cable, and another side is hinged with the chassis of STT prototype. Here, Axle pin tension sensor (XM-C82-10) and data-acquisition module (RM-4018V) were used to acquire drawbar pull force produced by STT prototype; and according to traveling speed, sampling frequency was set at 10 sample per second. After each drawbar pull test, the soil is thoroughly mixed with certain volumes of water by a deep scarifier and left to stand still for some days, till the soil residual shear stress meets the requirement of test.

It should be noted that it is impossible to carry out different tests under the same soil conditions. But for a comprehensive parameter (e.g. residual shear stress τ_{res}), it is not difficult to be reproduced within the allowable error range, and this provides the possibility for comparison tests. Here, the residual shear strength of bentonite-water mixture (τ_{res}) and the contact pressure (p_w) are selected as the experiment variables. The slip (i) and drawbar pull (F_D) are chosen as the performance values. It takes much time and effort to perform one drawbar pull test, so, according to typical working conditions, three sets of experimental variable combination are selected to conduct in this paper. The experimental variable combinations are shown in Table 5.

Before drawbar pull tests, the parameter values of pressure–sinkage relationship, k_c, k_ϕ and n, should be measured by situ pressure-sinkage test in the soil pool. But the test pool is relatively large, and it's very hard to keep soil homogeneous even if after repetitiously mixing. Therefore, multi-point testing was needed to evaluate the true situation of test soil. Here, six points were selected equidistantly along the moving direction of tracked walking mechanism to conduct situ tests, and the average values calculated with these tests were taken as the valid values to calculate draw bar pull. Experimental results obtained so far indicate that there is little difference between the values of k_c, k_ϕ and n obtained with different rectangular plates of high aspect ratios. The parameter values, measured from the pressure-sinkage situ tests with different residual shear stress of the test soil pool, are shown in Table 6.

3.3.3. Test results and discussion

As shown in Fig. 12, three drawbar pull tests were performed by the tracked walking mechanism of STT prototype with different values of experiment variables as shown in Table 5. The walking mechanism was kept moving uniformly in a straight line during the tests. The traveling distance is about 30 m. In order to eliminate interference of the motion

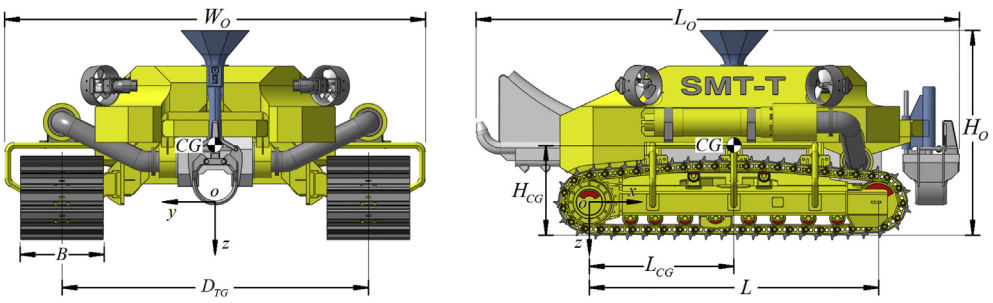

Fig. 10. Overview of the seafloor tracked trencher.

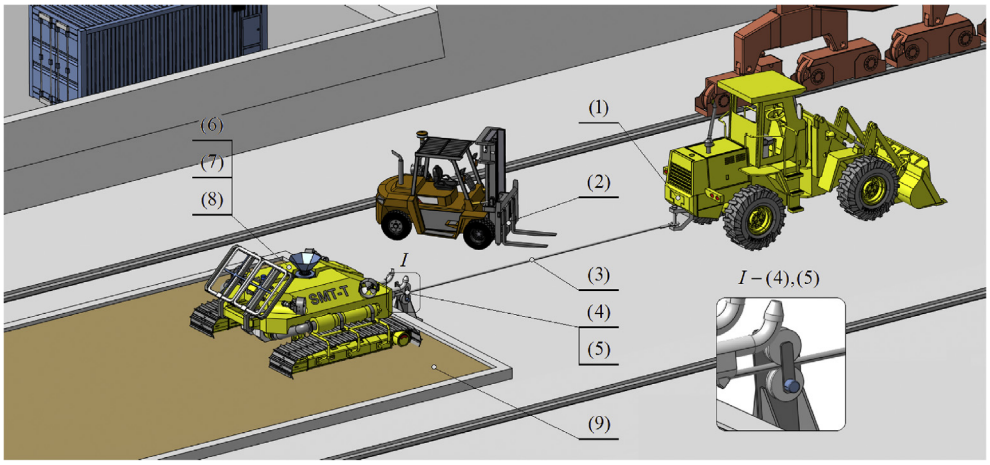

(1) Wheel loader; (2) Fork truck; (3) Towing cable; (4) Sensor support; (5) Cable length meters; (6) Seafloor tracked trencher; (7) Tension sensor; (8) Encoders fixed on rear sprockets; (9) Test soil pool;

Fig. 11. Schematic diagram of drawbar-pull test for STT.

Fig. 12. Drawbar pull test with tracked walking mechanism of STT prototype.

Table 3
General characteristics of STT prototype.

Overall dimensions	5.8 m(L_O) × 5 m(W$_O$) × 2.5 m(H_O)
Weight in air	20,000 kg
Weight in water	>5000 kg
Adjustment range of contact pressure (in water)	10–30 kPa
Walking mode	Tracked walking mechanism
Dredge mode	Jet trenching
Driving mode	Proportional hydraulic motor, Rear sprocket
Maximum velocity	0.5 m/s

Table 4
Principal dimensions of STT prototype.

	Symbol	Value	Unit
Width of track	B	1.2	m
Reference contact length with ground	L	3.5	m
Track gage	D_{TG}	3.7	m
Longitudinal center of gravity	L_{CG}	1.75	m
Vertical center of gravity	H_{CG}	1.1	m
Pitch circle diameter of sprocket	ϕ_S	0.64	m
Grouser Pitch	P_G	0.19	m
Grouser height	h	0.2	m

Table 5
Experimental variable combinations.

Test no.	Residual shear stress τ_{res} (kPa)		Contact pressure p_w (kPa)		Width of track B (m)	Grouser height h (m)
	Preset value	Actual value	Preset value	Actual value		
1	5.0	5.21	5	5.05	1.2	0.2
2	10	10.74	15	15.1	1.2	0.2
3	15	15.53	25	25.2	1.2	0.2

state change to the measured values of drawbar pull, the acceleration phase and deceleration phase were excluded in test data analysis. Valid range of test data was selected from 5 to 25 m. Measured values F_{DM} and mean values $\overline{F}_{DM}$ are shown in Figs. 13–15. Within valid range of traveling distance, the average slip i is approximate to a constant value, and the mean value $\overline{i}_{av}$ can be calculated with the data obtained from encoders. According to SSP model (Eq. (1)), with the drawbar pull prediction model (Eqs. ((4), (8), (9), (13) and (16)) and the parameter values obtained from the shear stress-displacement tests and pressure sinkage tests (Tables 2 and 6), the drawbar pull calculated values F_{DC} are drawn in Figs. 13–15 for comparison.

As shown in Table 7, the drawbar pull relative errors of the mean effective values obtained from tests to calculated values according to the SSP model were 15.47%, 11.61% and 9.72%

Table 6
Pressure-sinkage parameter values of the test soil pool.

Parameter	Test 1 (τ_{res1} = 5.21 kPa)	Test 2 (τ_{res2} = 10.42 kPa)	Test 3 (τ_{res3} = 15.53 kPa)
Cohesive soil modulus k_c (kN/m^{n+1})	1.92	4.25	8.71
Friction soil modulus k_ϕ (kN/m^{n+2})	3.57	8.43	13.24
Dimensionless exponent n	0.574	0.592	0.611

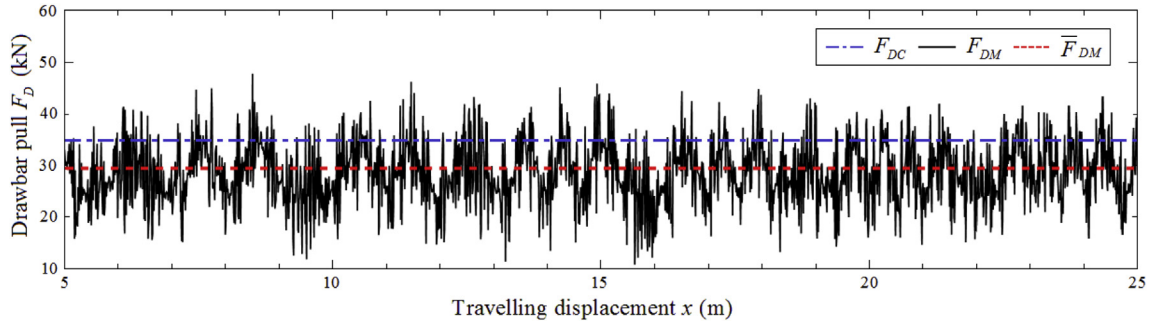

Fig. 13. Test 1 result in comparison with the calculated values according to SSP model (τ_{res} = 5.21 kPa, p_w = 5.05 kPa, h = 0.2 m, v_t = 0.358 m/s).

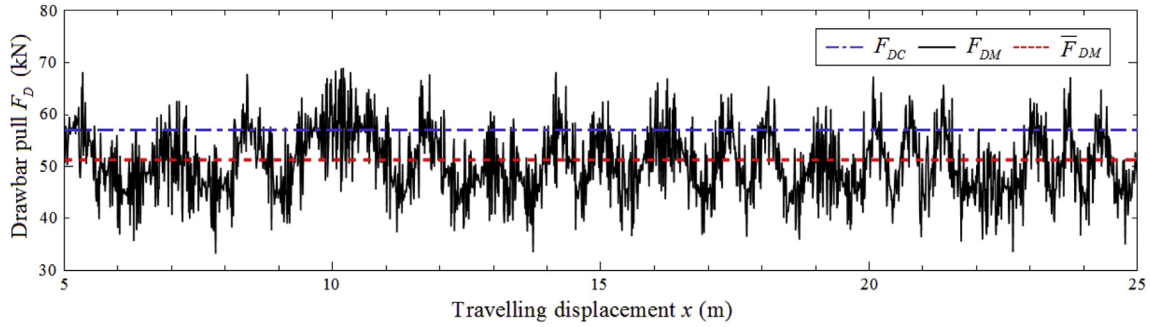

Fig. 14. Test 2 result in comparison with the calculated values according to SSP model (τ_{res} = 10.74 kPa, p_w = 15.1 kPa, h = 0.2 m, v_t = 0.319 m/s).

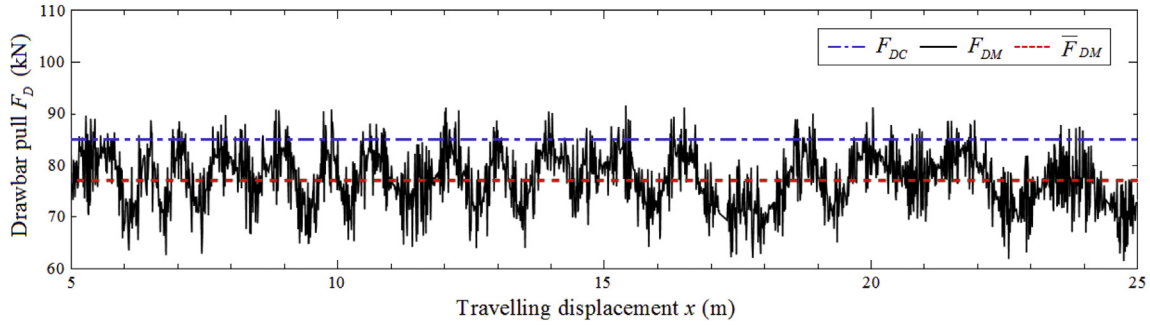

Fig. 15. Test 3 result in comparison with the calculated values according to SSP model (τ_{res} = 15.53 kPa, p_w = 25.2 kPa, h = 0.2 m, v_t = 0.337 m/s).

respectively (Figs. 13–15). The causes of relative error are numerous. On the one hand, the test soil pool is relatively large and it's very hard to stir and flatten test soil for each test, and the distribution of soil grains cannot be well-distributed in the test pool. On the other hand, the soil shear strength was controlled by water content, and should be maintained uniformity; but in actual operation, it is impossible to keep shear strength well-distributed. After mixing soil with water, the heterogeneity of viscosity-plasticity process of soil under self-weight is an important source of the relative differences. Of course, the reliability and error of test equipment (including measuring device) may be an important factor for the end of test; it can be found that the measured values were invalid or lost during the testing process.

Table 7
Performance values obtained from tests and relative errors.

Test no.	Slip ($\bar{i}_{av}$)	Drawbar pull F_D(kN)		Relative error ($\lvert F_{DC} - \overline{F}_{DM}\rvert / F_{DC} \times 100\%$)
		Calculated value (F_{DC})	Mean of measured values ($\overline{F}_{DM}$)	
1	0.311	34.89	29.49	15.47
2	0.244	58.47	51.68	11.61
3	0.173	85.35	77.05	9.72

But in general, by comparing the calculated values with the measured values from the verification tests shown in Table 7, the discrepancy of the values calculated by the prediction model is within allowable range; so, for STT prototype, the drawbar pull prediction model on the basis of the SSP model is feasible and effective. And this conclusion, from another side, also proved that the SSP model is effective.

4. Conclusions

(1) The shear stress-displacement relationship model of soil is very important to predict the tractive performance of

tracked vehicle. The existing shear stress-displacement models were proposed mainly for the terrestrial field of terramechanics. They may not be suit for the soft seafloor soil with flow surface and high water content. On the basis of track segment shear tests and comprehensive analysis of the shear deformation of the seafloor soil simulacrum (bentonite water mixture), a saturated soft-plastic soil shear stress-displacement model (SSP model) was proposed. Series of track segment shear tests were carried out. Results of the tests indicate that the SSP model could describe the behavior of track segment with good approximation.

(2) Through analyzing the main external forces, including environmental loads from seafloor soil and current applied to STT during the uniform trenching process in a straight line, drawbar pull prediction model was deduced based on the SSP model. A tracked walking mechanism of the STT prototype was built, and the verification tests for drawbar pull prediction model were designed and carried out. Results of the verification tests indicate that the discrepancy of the prediction values is within allowable range; the drawbar pull prediction model was feasible and effective. From another side, the drawbar pull tests verified once more that the SSP model is valid.

References

Baladi, G.Y., Rohani, B., 1978. A mathematical model of terrain vehicle interaction for predicting the steering performance of track-laying vehicles. In: Proc. of the 6th ISTVS Conference, pp. 285–332.

Bekker, M.G., 1960. Off the Road Locomotion: Research and Developments in Terramechanics. University of Michigan Press, Ann Arbor, MI, pp. 103–141.

Bekker, M.G., 1969. Introduction to Terrain-vehicle Systems. University of Michigan Press, Ann Arbor, MI, pp. 338–371.

Enderby, A.L., 1974. Deep-sea Sediments: Physical Mechanical Properties. Plenum Publ. Corp., New York.

Janosi, Z., Hanamoto, B., 1961. The analytical determination of drawbar pull as a function of slip for tracked vehicles in deformable soils. In: Proc. of the First Int. Conf. on Terrain-vehicle Systems. Turin, Italy.

Kim, H.-W., Hong, S., Choi, J.-S., 2005. Dynamic analysis of underwater tracked vehicle on extremely soft soil by using euler parameters. In: Proceedings of the Sixth ISOPE Ocean Mining Symposium, Changsha, Hunan, China, pp. 362–375.

Kitano, M., Jyozaki, H., 1976. A theoretical analysis of steerability of tracked vehicle. J. Terramechanics 13 (4), 241–258.

Li, L.I., Shulin, L.I., 2010. Simulation and mechanical characteristics of terramechanics of the surface soil on deep-sea bed. Eng. Mech. 27 (11), 213–220 (in Chinese).

Reece, A.R., 1965. Principles of soil-vehicle mechanics. Proc. Inst. Mech. Eng. Automob. Div. 180 (1), 45–66.

Royal Haskoning and BOMEL Ltd, 2008. Review of Cabling Techniques and Enviromental Effects Applicable to the Offshore Wind Farm Industry. Department for Business Enterprise & Regulatory Reform, UK.

Schulte, E., Handschuh, R., Schwarz, W., et al., 2001. Transferability of soil mechanical parameters to traction potential calculation of a tracked vehicle. In: Proceedings of the 5th ISOPE Ocean Mining Symposium, Tsukuba, Japan, pp. 123–131.

Upadhyaya, S.K., Wulfsohn, D., Jubbal, G., et al., 1989. Traction prediction equations for radial ply tires. J. Terramechanics 26 (2), 149–175.

Watanabe, K., Kitano, M., 1986. Study on steerability of articulated tracked vehicles – Part 1. Theoretical and experimental analysis. J. Terramechanics 23 (2), 69–83.

Wong, J.Y., Preston-Thomas, J., 1983. On the characterization of the shear stress-displacement relationship of Terrain. J. Terramechanics 19 (4), 221–232.

Wu, H.Y., He, J.S., 2010. Establishment of the deep-sea soft sediments shearing strength – shear displacement model. Mod. Appl. Sci. 4 (1), 21–27.